Proceedings of the Institution of Mechanical Engineers, Part G: Journal of Aerospace Engineering,
2016, Vol 231, Issue 8, pp. 1369 - 1390. DOI: 10.1177/0954410016651294

Numerical Simulation of the Airflow Over a Military Aircraft with Active Intake

T Triantafyllou*, T Nikolaidis, M Diakostefanis, P Pilidis
Cranfield University, School of Aerospace, Transport and Manufacturing, College Rd, Cranfield, Bedford MK43 0AL, United Kingdom

ABSTRACT

The aim of the study presented herein is to numerically predict the behaviour of the airflow around a flying military aircraft with an active intake in which the airflow may enter and travel all the way up to the Aerodynamic Interface Plane (AIP, the analytical interface between the inlet and engine). Computational Fluid Dynamics (CFD) is used as the basic tool. The geometry created consists of a full scale military aircraft exposed to different flight conditions. The flow results are mainly focused at the AIP since the present study is a part of a greater research effort to estimate how the airflow distortion induced to the engine's face due to the aircraft's flight attitude, affects the embedded gas turbine's performance. The obtained results were validated through a direct comparison against similar experimental ones, collected from a wind tunnel environment.

KEYWORDS
Computational Fluid Dynamics, Aerodynamic Interface Plane, Gas Turbine Performance, Aircraft Intake System, Airflow Distortion

NOMENCLATURE

Symbols

A [m2]	Cross Sectional Area
c_p [-]	Static Pressure Coefficient
c_P [-]	Total Pressure Coefficient
D or d [m]	Diameter
I [%]	Turbulence Intensity
k [J/Kgr]	Turbulent Kinetic Energy
M [-]	Mach Number
P [Pa]	Total Pressure
p [Pa]	Static Pressure
R [J/KgrxK]	Gas Constant
Re [-]	Reynolds Number
T [K]	Total Temperature
t [K]	Static Temperature
u [m/s]	Velocity
W [Kgr/s]	Mass Flow Rate
y+[-]	Dimensionless Wall Distance

Greek Symbols

*Corresponding author: Cranfield University,
Propulsion Engineering Centre,
Cranfield, Bedfordshire, UK
email: t.triantafillou@cranfield.ac.uk

γ [-] Ratio of Specific Heats
Δ [-] Difference
ε [J/Kgrxs] Turbulence Dissipation Rate
ρ [Kgr/m^3] Density

Abbreviations

AIP Aerodynamic Interface Plane
AOA Angle of attack
AOSS Angle of Side Slip
CFD Computational Fluid Dynamics
CM Corrected Massflow
DP Design Point
FS Fuselage Station
NDMF Non Dimensional Mass Flow
OD Off Design
OPR Overall pressure Ratio
PRF Pressure Recovery Factor
PR Pressure Ratio
PW Pratt & Whitney
RNG Re-normalization Group
SLS Sea Level Static
SST Shear-Stress Transport
TET Turbine Entry Temperature

1. INTRODUCTION

In air vehicle design and in the study of flow phenomena in general, Computational Fluid Dynamics (CFD) is a really powerful tool. It provides a means of predicting the flow behaviour around a novel design even at the phase of its conceptual design and before any actual structure is created. In that way new designs are judged based on CFD results at a relatively low cost and many of the actual tests have been replaced by CFD simulations.

In CFD, the set of basic equations that govern fluid flow are discretized and solved numerically within a finite computational domain. FLUENT (1), a commercial CFD solver based on finite volume methodology (FVM) was used throughout the present study at its steady state and density based options and the turbulence model selected was the realizable version of the k-ε turbulence model.

The selected geometry model comprises of a full scale military aircraft which was tested in 27 different flight conditions at 20000ft altitude. It is a 3-dimensional geometry inspired by a General Dynamics/Lockheed Martin F-16 fighter aircraft and it contains the entire airframe including the intake.

For the tested flight attitudes a combination of different Angles of Attack (AOA) and Angles of Sideslip (AOSS) was selected in the range of 0 to 16 degrees each, in three different flight Mach numbers, namely flights at 0.35M, 0.6M and 0.85M. The main objective of this analysis is to get a full (3-D) representation of the flow reaching the engine. Based on this representation the effect of distorted flow on the engine's performance may be studied.

In the gas turbine performance calculations an engine inspired by the Pratt and Whitney F100-PW-229 engine was used as a baseline. The effects of the engine in the simulation model were implied through the definition of boundary conditions at its inlet and outlet. The space in between

is hollow since the addition of the engine in detail from its FAN inlet to its nozzle exit would have rendered the computational cost of its numerical solution unaffordable.

In the definition of the boundary conditions and specificaly whenever the performance of the engine needeed to be simulated this was accomplished using the TURBOMATCH scheme. This is a Cranfield University gas turbine engine simulation software, which was developed by Palmer[2] and it facilitates design point (DP), off-design (OD) and transient operation performance calculations for aero (civil and military) and industrial engines. Turbomatch program has been used for Cranfield's research activities and it has been proven reliable, accurate, and extremely flexible.

The obtained CFD results were validated through a direct comparison against similar experimental ones collected from a wind tunnel environment. More specifically the static pressure coefficients measured at specific stations of the aircraft's structure with reference to the free stream conditions are in good agreement when compared against similar experimental results obtained in a wind tunnel environment [3].

The present work has gone a bit further than those of Huband et al[3] and Reue et al [4] in that the flow results refer to a full scale military aircraft geometry which has a fully active intake. This exact configuration provides a means of collecting airflow distortion data at the engine's face.

2. AIRCRAFT GEOMETRY

The first challenging part in the progress of the present work was the creation of a reliable geometry, capable of capturing the desired flow effects.

The geometry model was created from scratch combining information found in the open literature (text books and on line).

First a drawing with some cut views at different locations of the aircraft was come across in [5] and the general dimensions of the airframe, like its length, height and span, were located in [6]. Figure 1 presents an overview of these cut views.

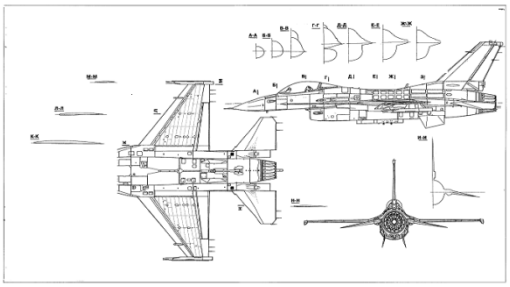

Fig. 1 General Cutviews of a Millitary Aircraft's Geometry [5]

These views were then digitized with the aid of the XY extract [7] and translated into point coordinates, having always in mind that every cut view should be scaled accordingly to comply with the general dimensions of the aircraft. The acquired data, were imported in a .txt format into GAMBIT [8] which is a pre-processor for geometry modelling and mesh

generation from the FLUENT family of software products. In the next step the created geometry in GAMBIT, comprising only from points, was exported in an IGES format and imported into ICEM CFD which also deals with the creation of model geometries in the pre-processing phase of studying flow phenomena. Lines connecting these points and surfaces oriented by these lines were created having as a target ''a water tight'' geometry.

2.1 Intake

Along with the airframe, the model geometry has an active intake in that the air may flow all the way up to the engine's face. The geometric features of the intake that needed to be complied with in the creation of the simulation model, as described in [9] and presented in fig. 2, were the following:

- Its geometry is fixed without any movable parts.
- Its subsonic part is a diffusive duct with a gradually increasing cross section from the throat to the exit.
- At the inlet the lower lip is blunt, while the upper is sharp.
- There is a 10in long splitter plate at the beginning of the intake which extends from the upper lip towards the nose of the aircraft.
- The intake is separated by the fuselage by a 3.3in diverter.

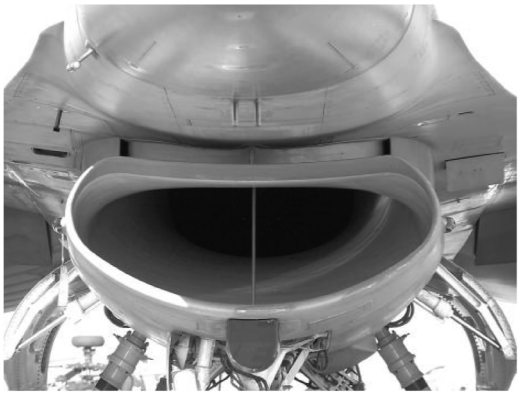

Fig. 2 Fixed Geometry Intake on the General Dynamics/Lockheed Martin F-16[10]

The position and the basic shape of the intake were both implied by the surrounding airframe structure. What needed to be considered though were

- the size of the throat area
- the rate of diffusion for the cross sectional areas from the throat to its exit, and
- the size of the outlet area at the engine's face.

These parameters had to be defined in such a way so that the mass flow allowed to pass through the intake matched the demands of the gas turbine engine at the desired flight conditions.

In cases where the intake geometry is fixed, like the one studied in the present work, this matching process becomes more challenging, because the same geometry needs to provide the engine with the desired mass flow in the entire operating envelope.

The fixed intake throat was sized to accommodate the maximum engine corrected airflow at a throat Mach number of 0.75 [9]. This condition was

assumed that happens when the aircraft flies at a high subsonic Mach number (≈0.9) and at a high altitude (at the tropopause, around 37000ft altitude). Running in TURBOMATCH the performance simulation model for the baseline engine [11] at the above conditions, resulted in getting the desired by the engine mass flow.

Taking into account that at the engine's face the flow is subsonic about 0.48M [9], the sizing process of the intake could proceed. The thermodynamic parameters (total and static temperature, total and static pressure) were based on an assumed 0.95 intake pressure recovery, a value that is within the typical range for subsonic flows [12].

Having all these data, the key geometric features of the intake geometry like its cross sectional areas at the throat and the outlet were both calculated by using the 'Q-function' [13] This parameter relates the Mach number (M) with the cross sectional area at a specific point (A) , given the mass flow rate (W) and the total pressure (P) and temperature (T) at this point.

$$Q = \frac{W\sqrt{T}}{AP} = \sqrt{\frac{\gamma}{R}} \times \frac{M\alpha}{\left(1 + \frac{\gamma - 1}{2} M\alpha^2\right)^{\frac{\gamma+1}{2\times(\gamma-1)}}} \qquad \text{(eq.1)}$$

The resulted intake geometry with its gradual growth of the intake cross sectional area from the throat to the outlet is presented in fig. 3 below. Similarities can be observed with the respective area distribution of a military aircraft [9], as it is presented in fig. 4, giving thus some credits to the created geometry.

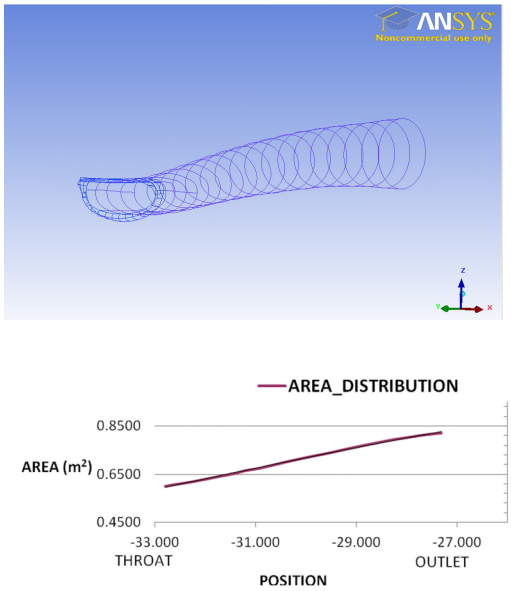

Fig. 3 Intake Cross Sectional Area Distribution

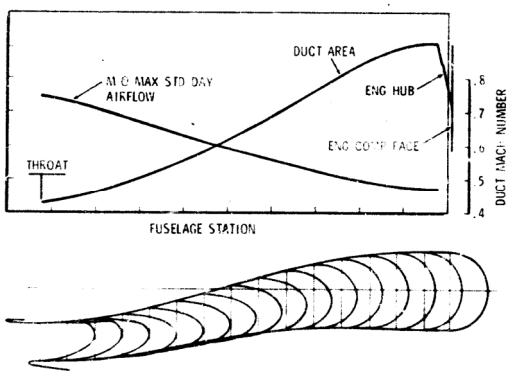

Fig. 4 YF-16 Subsonic Duct Geometry and Area Distribution [9]

3. MESH GENERATION

Once the geometry model was created the next steps in the process of setting up the numerical solution were first the definition and then the meshing of the flow region (computational domain).

The domain selected in the present work has a bullet shape comprising of a hemisphere and a cylinder. The radius of the hemisphere is about 12 times the length of the aircraft (=180m) and the length of the cylinder is more than 15 times the length of the aircraft (=250m). The aircraft model is placed inside that domain closer to its front part (in the hemisphere) leaving enough space for the exhaust gases to sufficiently adapt with the surrounding undisturbed conditions before they reach the domain's boundary.

The computational domain's size was a compromise between computational cost and accuracy. On one hand the domain should have been big enough to allow the flow dynamics to be fully developed but on the other hand it should have been kept at a manageable size so that it could have been handled by the capabilities of the solving processor.

The creation of an unstructured mesh was preferred mainly due to the complexity of the model's geometry. The mesh was generated in ICEM CFD following a bottom up approach. Starting from a water tight geometry which is a prerequisite for a successful mesh generation process, a surface mesh was created on the aircraft (fig. 5). The maximum curve size for each surface line was specified in such a way aiming first to avoid the creation of highly skewed elements and at the same time to generate a more fine mesh at the areas of higher interest (like inside the intake where the airflow distortion data needed to be collected).

The volume mesh, a cutview of which is presented in fig. 6, comprised of tetrahedral elements created following a Delaunay algorithm. In Delaunay meshing the general idea is to form a mesh where each triangle's three points lie on the edge of a circle that doesn't contain any other point[(14)]. This forces the mesh to have triangles that tend to be as close to evenly spaced as possible which helps to avoid highly skewed elements.

The size of the tetra elements created to cover a volume is implied by the mesh settings applied to the surrounding surfaces. Wherever there is a need for extra refinement a grid density can be applied. In the present study such densities were introduced inside the intake and behind the exhaust nozzle.

Finally, 13 prism layers were created adjacent to all the wall surfaces to capture the boundary layer effects. The selected parameters were based on a Y+ value in the log-law region (30-300) and the height of the first node was set to 0.001m from the surface, relying on the wall functions of the chosen turbulence model to capture the space in between.

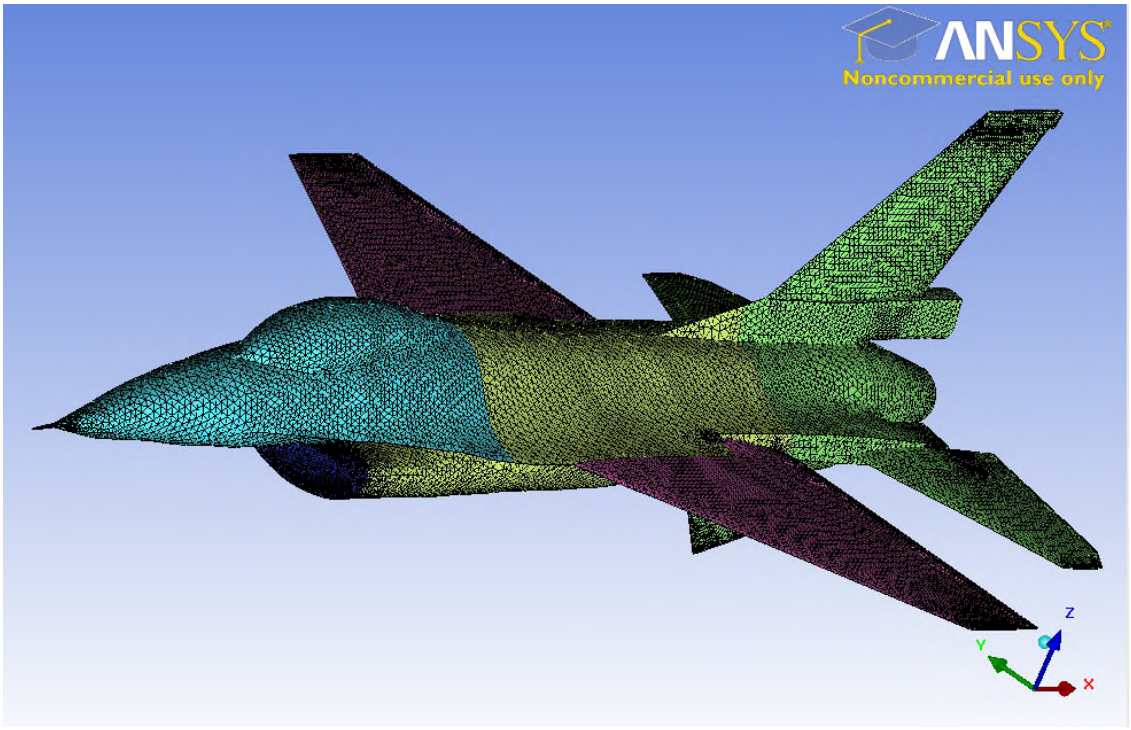

Fig. 5 Surface Mesh on the Aircraft's Geometry

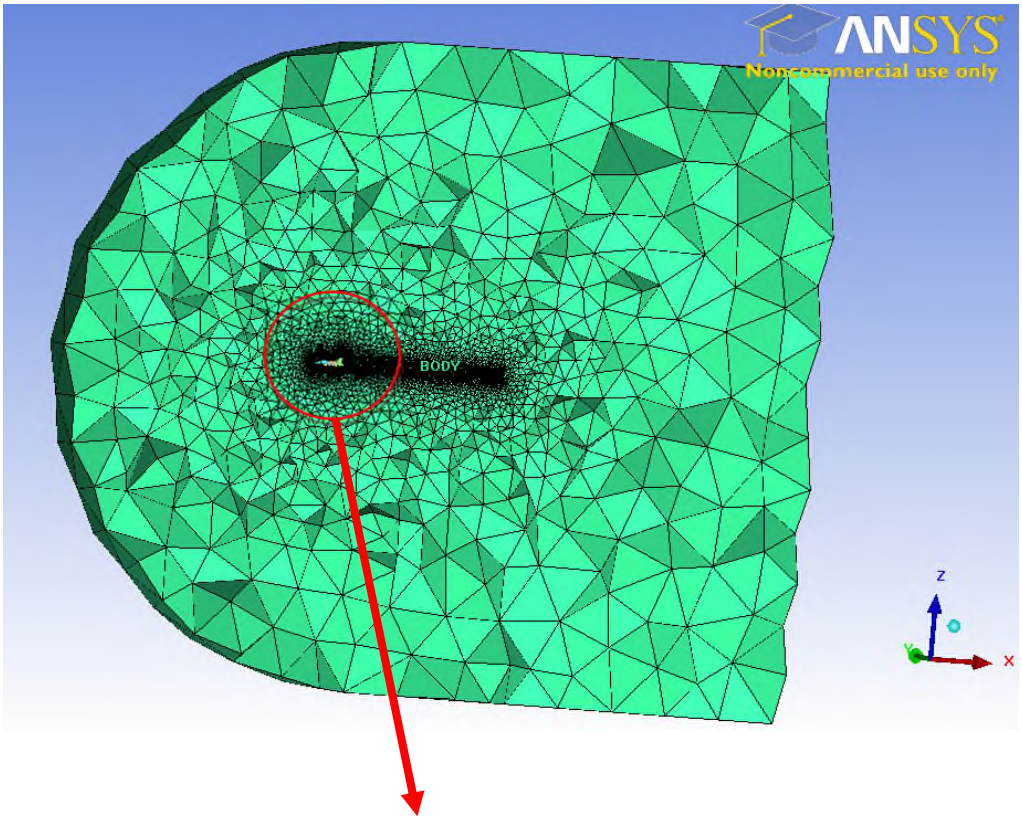

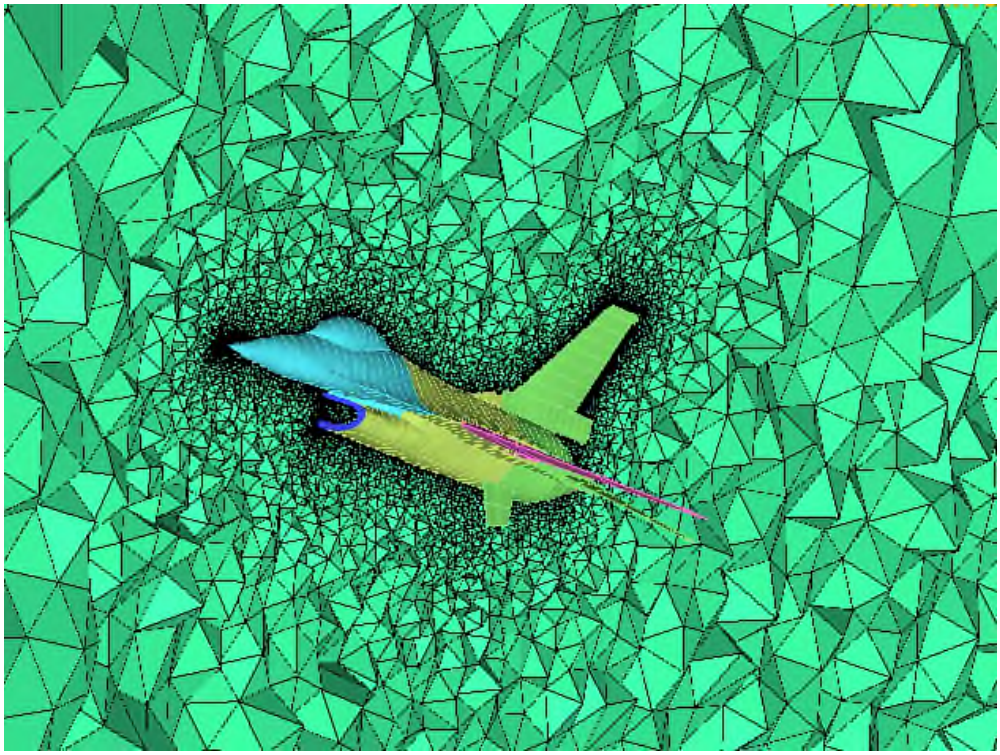

Fig. 6 Cutview of the Volume Mesh

Mesh structures of different sizes were developed to eradicate mesh dependency of the solution. Four different grids were used to simulate a 0˚ AOA and 0˚ AOSS flight scenario at 0.6M speed. In all cases the computational solutions were obtained by solving the Reynolds averaged Navier–Stokes equations amended by those implied from the standard k–ε turbulence model with standard wall functions. The methodology followed aimed to quantify the mesh dependencies by monitoring some basic flow parameters, like the mass flow rate at the intake's exit and the area weighted flow velocity magnitude at the same plane.

These numerically predicted parameters were graphed against the number of the cells of each of the above tested grids. The resulted graphs are presented on figs 7 and 8 respectively.

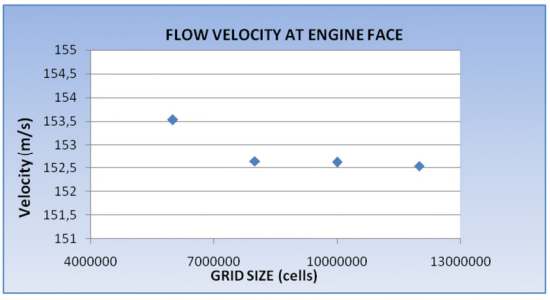

Fig. 7 Influence of Grid Size on Monitored Flow Velocity at Engine's Face

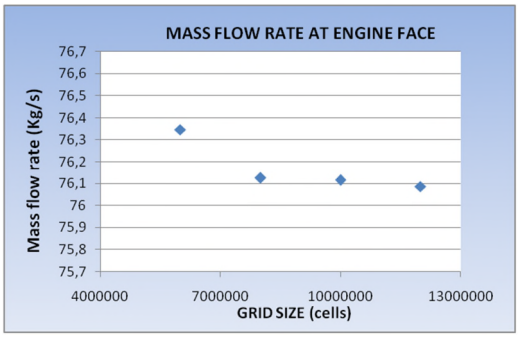

Fig. 8 Influence of Grid Size on Monitored Mass Flow Rate at Engine Face

Looking at the above figures it is clearly revealed that grids consisting of more than 8 million cells are in the asymptotic region. As such, the usage of grids of that size is a good compromise between affordable computational cost and acceptable numerical uncertainty. Based on that, the simulations required by the present study were run utilizing 10 million cell models.

4. BOUNDARY CONDITIONS

The boundary conditions augment the differential equations to completely determine the solution. As it can be seen in fig 9, boundary conditions have been set,

- at the boundaries of the entire domain,
- at the intake's exit,
- at the engine nozzle's exit and
- at the solid walls of the geometry.

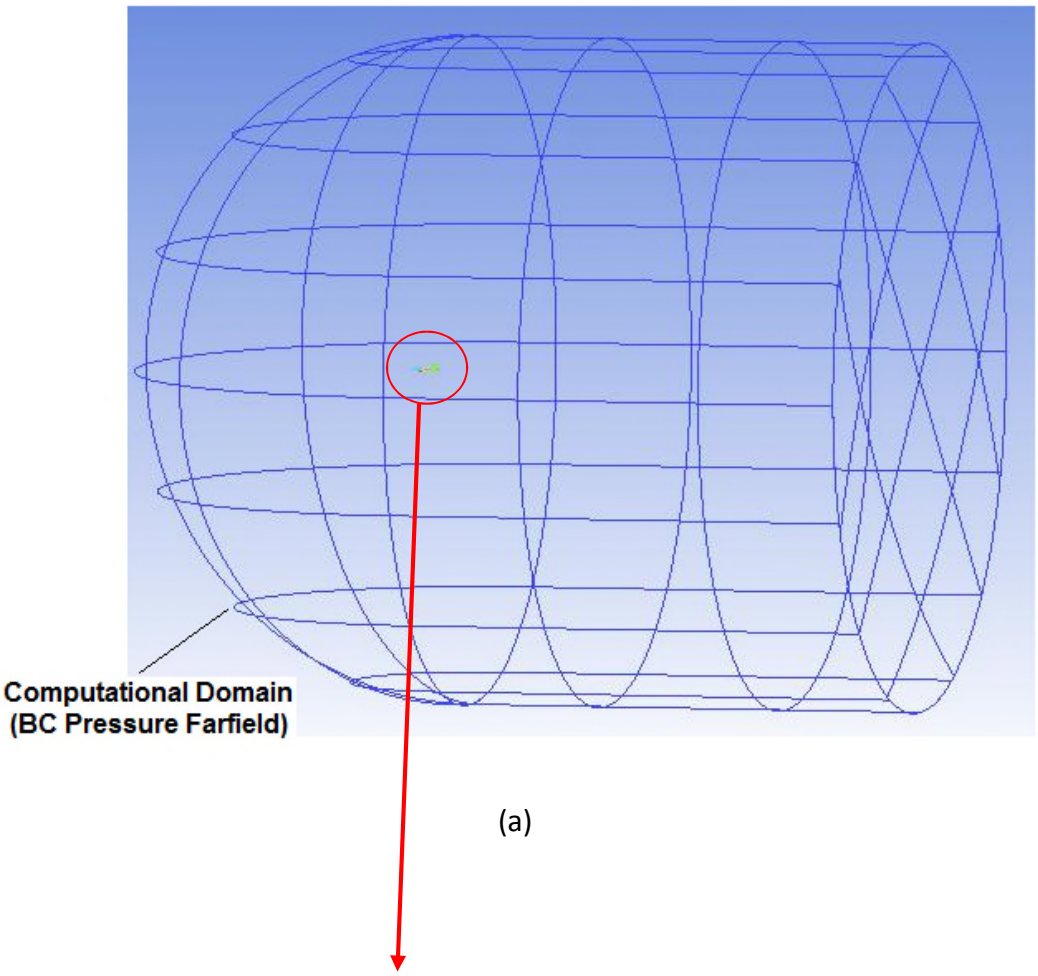

(a)

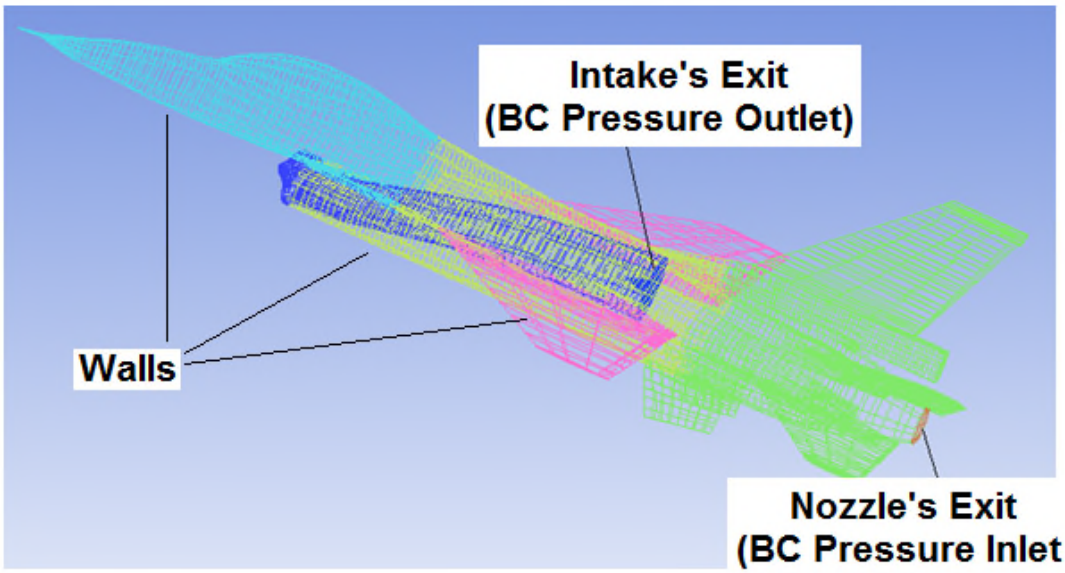

(b)

Fig. 9 Boundaries of the Computational Domain

The outer boundaries of the entire computational domain [fig 9 (a)] were defined as pressure far field and the flight conditions of the aircraft were defined through the settings of Mach number and direction of the incoming flow. At the examined altitude of 20000ft the ambient conditions of pressure and temperature are 46557 Pa and 248.5 K respectively [15].

To complete the boundary condition settings with specifying the transported turbulence quantities, the turbulence intensity was set to 2% since the flow at this point is expected to be moderately turbulent and the hydraulic diameter was set to 360m, considering the cross sectional area of the domain. The turbulence intensity, I, is defined as the ratio of the root-mean-square of the velocity fluctuations, u', to the mean flow velocity u_{aver}. A turbulence intensity of 1% or less is generally considered low and turbulence intensities greater than 10% are considered high [1].

Inside the Computational Domain, on the aircraft's geometry, the intake's exit and the nozzle's exit are respectively outlet and inlet boundaries (fig 9) and the condition's applied at these boundaries denote the presence of the gas turbine in the domain.

Since flow results at the intake's exit are of increased importance for the present study it was decided not to impose explicit boundary conditions at that plane. Instead, a simple

accelerating duct (with a decreasing cross sectional area to the direction of the flow) was added behind that plane, as shown in fig 10. Inside that duct it was assumed that neither pressure losses nor work additions take place. By extending the flow region in that way the flow was freely expressed at the plane of interest i.e. the boundary of the domain had been moved downstream and the conditions imposed at that point did not directly interfere with the flow results at the AIP.

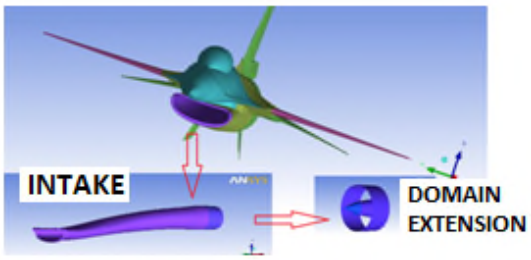

Fig. 10 Computational Domain's Extension Behind the AIP

The boundary condition at the exit of that duct was set as pressure outlet. To complete the settings at that boundary, the value of Static Pressure needed to be specified at this point. This value in the simulation process creates sufficient ''sucking conditions'' at the intake's exit and in conjunction with the flight Mach number they both define the mass flow rate that will finally enter the intake.

The required static pressure at this point was the result of an interaction between TURBOMATCH and CFD. One of the prerequisites for this assessment was to create the baseline engine's performance simulation model.

The model's parameters, e.g. FAN pressure ratio, overall pressure ratio, bypass ratio, TET, were based on information found in the open literature [16], [17]. As for the important parameters that we did not have any information about, e.g. component effeciencies, pressure losses, cooling flows, these were continously adjusted, through engineering judgments and optimization techniques, in order to match the engine's DP known output (net thrust and SFC).

Consequently, an engine with performance closely approximating that of F100-PW-229 engine was finally modelled. Table 1 presents the baseline engine's design point performance data that were used for the validation of the performance simulation model.

Table 1 The F100-PW-229 Engine's Design Point Performance Data [16], [17]

Dry Thrust (Nt)	79200
SFC (lb/hr/lbf)	0.74
Dry Fuel Flow (Kgr/s)	1.67

Using the engine's performance simulation model a design point run at Sea level Static (SLS) conditions was conducted in TURBOMATCH. Then three off design cases were also run simulating the operation of the engine

at 0.35M, 0.6M and 0.85M flights at 20000ft altitude.

In these performance calculations the FAN rotational speed (PCN) was used as the driving parameter and its value was progressively adjusted until for each condition the resulted mass flow entering the engine, corresponded to the 100% of the design corrected airflow (CM).

The rationale underlying this selection was to create the same inflow conditions in all cases, for comparison purposes.

The resulted mass flow rates were used then in CFD as target values and the static pressure at the intake's exit was respectively adjusted so as to match the mass flow rate values in TURBOMATCH. The resulted values of static pressures were the following:

- 40679 Pa at 0.35M
- 48000 Pa at 0.6M
- 60200 Pa at 0.85M

From the TURBOMATCH results the Total Temperatures at the same plane (intake's exit) were the following

- 255K at 0.35M
- 266K at 0.6M
- 284K at 0.85M

These temperature values were also introduced in CFD as temperature boundary condition settings.

To complete the boundary condition settings at the intake's exit the turbulence intensity was set to 7% since the upstream flow is considered quite turbulent and the hydraulic diameter was set to 0.961m taking into consideration the cross sectional area of the intake.

The engine's nozzle exit was defined as pressure inlet. The required Total Pressure and Temperature at this point were resulted from the TURBOMATCH simulation runs for the three off design cases (0.35M, 0.6M and 0.85M flights at 20000ft altitude). The resulted values were the following

- 151987 Pa and 780K for the 0.35M flight
- 180359 Pa and 816K for the 0.6M flight
- 225418 Pa and 869K for the 0.85M flight

As for the static pressure its value was derived from the critical ratio of total to static pressure and based on a choked nozzle assumption.

$$\frac{P}{p} = \left(1 + \frac{\gamma - 1}{2} M^2\right)^{\frac{\gamma}{\gamma - 1}} = 1.85 \qquad \text{(eq. 2)}$$

The turbulence parameters at the engine's outlet were set at 8% and 0.583 for the turbulence intensity and hydraulic diameter respectively.

The whole process of defining the boundary conditions through the interaction between Turbomatch and CFD is summarized in the flow chart presented in fig. 11.

Finally, all the solid surfaces were defined as stationary walls with no slip as shear condition.

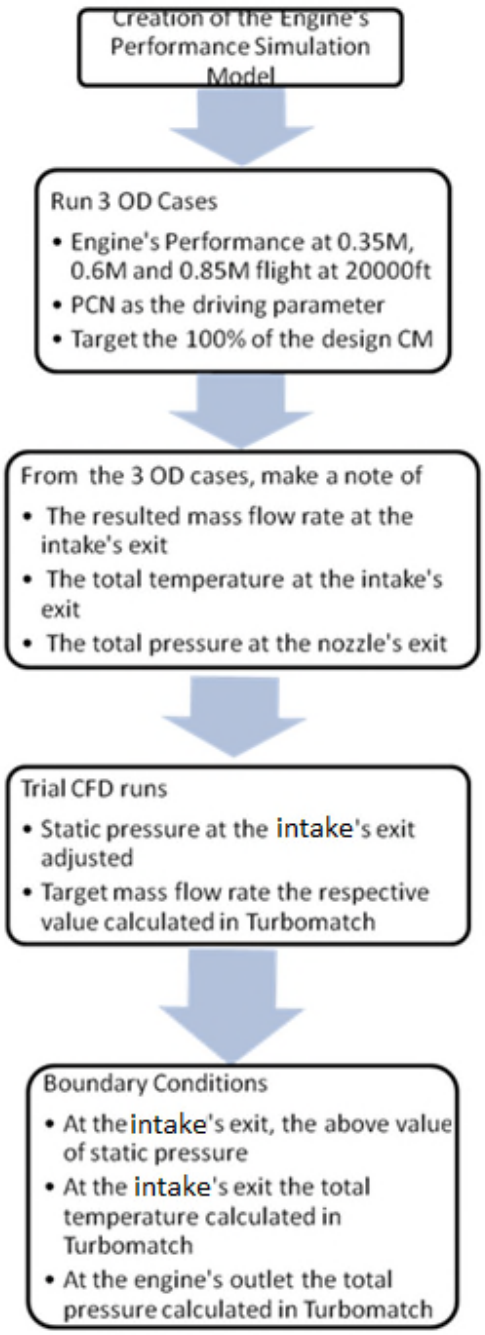

Fig. 11 The Process of Defining the Static Pressure at the INTAKE's Exit.

5. NUMERICAL SIMULATION

5.1 Turbulence Model Dependency Study

The selection of the Turbulence model plays significant role in numerical simulations since the successful modelling of the turbulent flow greatly increases the quality of the acquired solution. In the present study wall Turbulence and free Turbulence were expected to occur.

The prism layers of the created mesh, for capturing the boundary layer effect, were built based on a Y+ value greater than 30. That means that the first node of the grid, next to the walls, was placed in a considerable distance from them (log-law layer) and as such a turbulence model with wall functions needed to bridge the flow results with the solution variables in the viscosity-affected area [18].

In order to examine any influence on the solution that the selection of the turbulence model may have had, three variants of the k-ε turbulence model were tested, namely the standard version, the k-ε RNG and the k-ε Realizable. These three models were qualified because all of them provide the option of wall functions.

These models were tested in two different flight conditions in order to duplicate any potential findings. Flight at 0.35M with 8^0 AOA and 8^0 AOSS was the first one, whereas flight at 0.85M with 8^0 AOA and 16^0 AOSS was the second one. The results obtained with the above Turbulence Models are resumed in figs 12 and 13, where the predicted Total Pressure distribution at the engine's face is shown.

Fig 12 reveals that the Total Pressure distribution differs depending on the utilized Turbulence Model. This statement duplicates its truth looking at fig 13, where again the visualized flow results show that the

total pressure distribution differs between the three selected turbulence models. In that figure it can be observed that both the RNG and the realizable variants of the k-ε turbulence model predict a low pressure area of about the same size at the 3 o'clock area of the engine's face plane. It is highly likely this low pressure area to occur at that location due to the increased value of the AOSS. The k-ε standard turbulence model though predicts a smoother variation of the total pressure at that area..

More quantitative difference among the examined models is observed when comparing predicted values of area weighted average total pressure and mass flow rate at the engine's face plane for the above referenced flight conditions. The results are shown in Table 2. The results, although they differ, they are really close to each other.

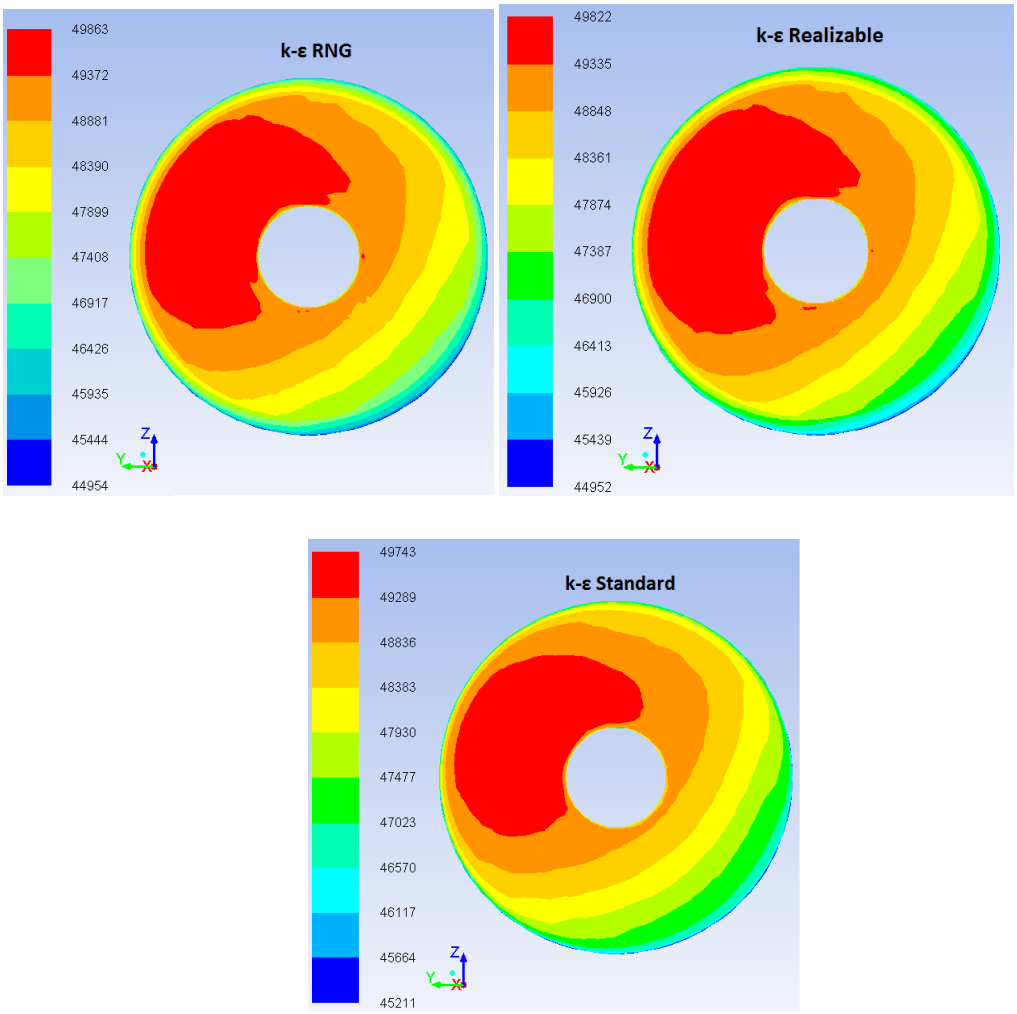

Fig. 12 Total Pressure (Pa) Contours at the Engine's Face with Varying the Turbulence Model-Flight at 0.35 with 8^0 AOA and 8^0 AOSS

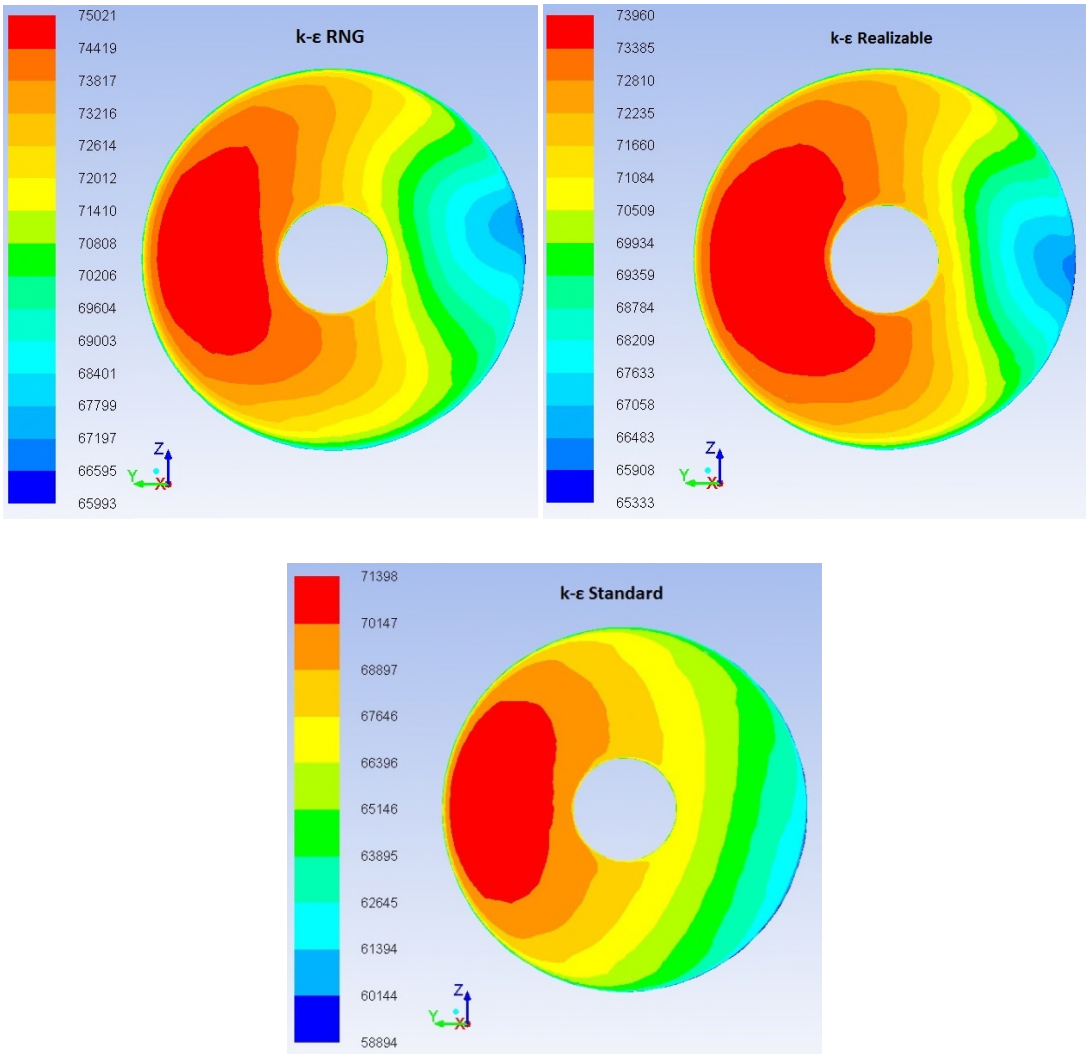

Fig. 13 Total Pressure Contours at the Engine's Face with Varying the Turbulence Model-Flight at 0.85 with 8^0 AOA and 16^0 AOSS

Table 2 Engine Face Results with Varying Turbulence Models

	At the Engine's Face			
	0.35M, 8^0 AOA and 8^0 AOSS		0.85M, 8^0 AOA and 16^0 AOSS	
Turbulence Model	**Area Weighted Average Total Pressure (Pa)**	**Mass Flow Rate (Kgr/s)**	**Area Weighted Average Total Pressure (Pa)**	**Mass Flow Rate (Kgr/s)**
k-ε standard	48613.68	56.67	71788.64	78.53
k-ε RNG	48677.46	56.14	72324.39	80.69
k-ε Realizable	48651.95	56.04	71670.71	78.69

Based on the above findings and having no other experimental data to validate the results and to clearly reject or support one of the three Turbulence Models, the k-ε Realizable variant was finally adopted since:

- it seems to be more accurate than the k-ε standard model since it predicted the low pressure area at 3 o'clock on the engine's face plane, for the flight attitude of 0.85M with 8^0 AOA and 16^0 AOSS which is highly likely to occur due to the increased AOSS,
- its usage is suggested by the ANSYS FLUENT when the case is finally checked before start iterating, and it is recommended for better prediction of the turbulent viscosity [(1)].
- this model is also likely to provide superior performance for flows involving rotation, boundary layers under strong adverse pressure gradients, separation, and recirculation [(1)], like the flow field inside the intake.

Another turbulence model considered was the k-omega SST one, which predicts with better accuracy flow cases where flow separations may occur [(19)]. This model though does not provide standard wall functions in FLUENT [(1)] and it uses enhanced wall functions as the near-wall treatment [(20)] . As such it needs the mesh to be fully refined near the walls (y+≈1). The complexity of the geometry in the present study though did not allow the usage of this model since such an action would have increased the already big size of the mesh and it would have made its solution computationally unaffordable.

5.2 Convergence Criteria

The convergence of the solution was assessed in two different ways. The first one was by progressively tracking the imbalances of the algebraic equations. The solution was considered converged when the residuals reached and stabilized at a low value in the order of 10^{-4}.

Along with examining the residuals two flow variables were also monitored in the progress of the solution namely the mass flow rate at the intake's exit and the flow velocity magnitude at the same plane. Solution was not considered converged not until these variables had been stabilized at a certain value that stayed unchanged in the progress of the solution iterations.

6. CFD VALIDATION

The numerical results referring to the external flowfield (around the entire aircraft) were validated through a comparison with [(3)] and [(4)]. The former describes a numerical solution based on a scaled F-16A model flying at 0.85M with 16.04˚ AOA whereas the latter gives out some experimental results from the same model exposed to the same flying conditions in a wind tunnel environment.

Figure 14 below directly compares the Static Pressure contours obtained numerically in the present study for

the flight scenario of 0.85M with 16˚ AOA and in [3].

As it can be clearly seen the contours present many similarities. In both cases the lowest pressure areas are predicted to occur at the wing roots and at the leading edges of the horizontal stabilizers. Looking closer at the values of Static pressure at these areas it can be clearly seen that they are very close to each other. For instance, the Static pressure at the wing root in the present study is predicted to be in the range of 9420 Pa which is really close to the 200 psf Static pressure that was predicted in [3] for the same area.

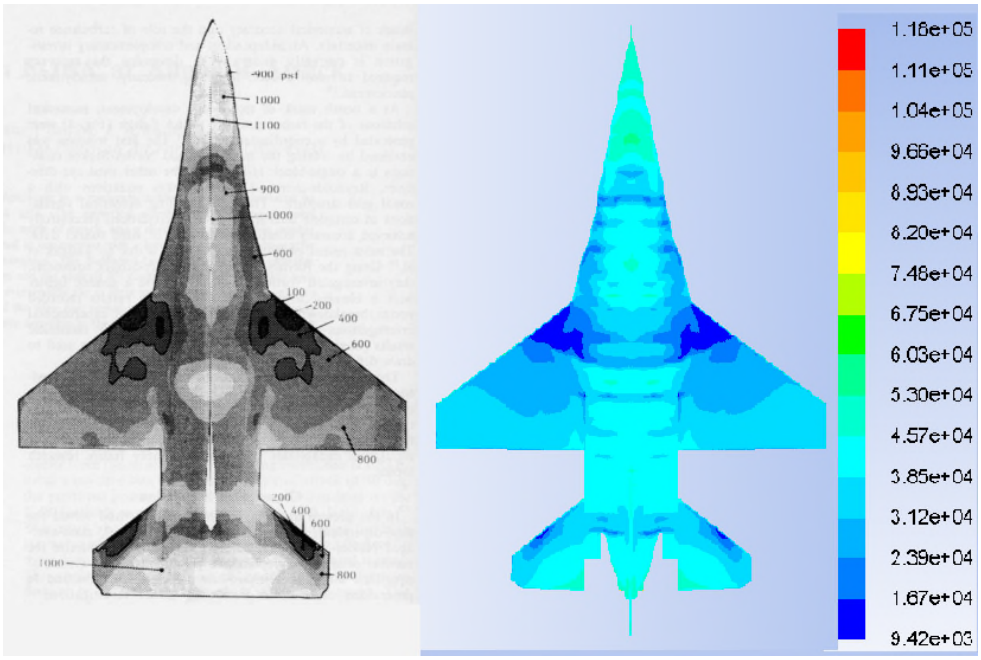

Fig. 14 Comparison of the Static Pressure Contours Obtained in my Case (on the Right) with those Quoted in [3] (on the Left) for the Flight Scenario of 0.85M with 16˚ AOA.

Specific values of pressure coefficients are stated in [4] which were based on actual measurements taken circumferentially at the planes 1, 2 and 3 depicted in fig 15. A direct comparison of these results with the respective ones calculated in the present study is presented in figs 16, 17 and 18. The compared results are again in a reasonable agreement.

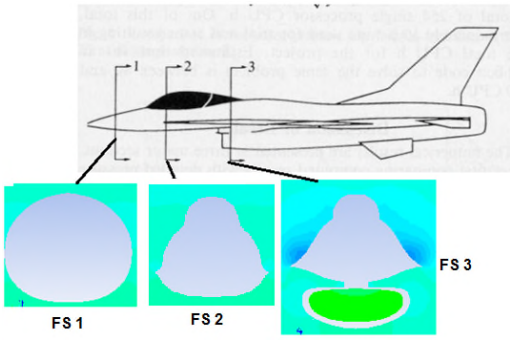

Fig. 15 Location of the Pressure Measurement Planes in Relation to the Entire Geometry

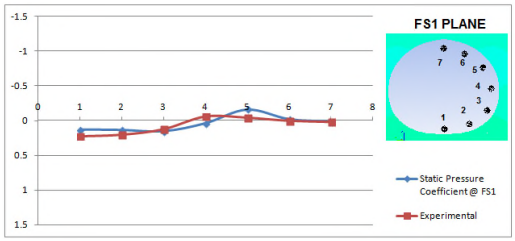

Fig. 16 Comparison with experimental Results [4] of the Static Pressure Coefficient at the Plane FS1 for 0.85M Flight and 16˚ AOA

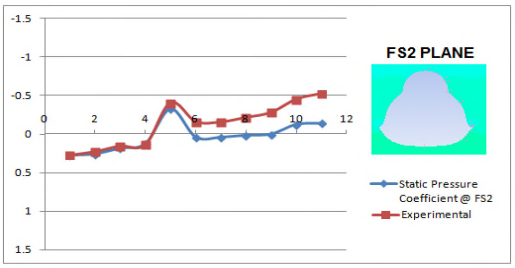

Fig. 17 Comparison with experimental Results [4] of the Static Pressure Coefficient at the Plane FS2 for 0.85M Flight and 16˚ AOA

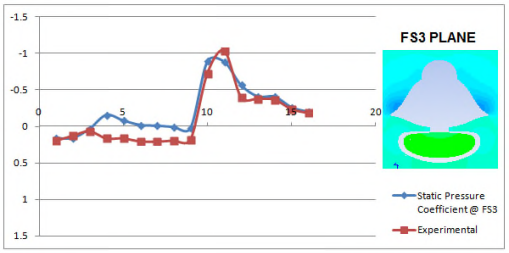

Fig. 18 Comparison with Experimental Results [4] of the Static Pressure Coefficient at the Plane FS 3 for 0.85M Flight and 16˚ AOA

7. RESULTS

The simulation model described in the previous sections, was tested in 27 different flight conditions. Three different flight Mach numbers with 9 different flight attitudes each. All the tested flight attitudes are presented in Table 3.

Table 3 Tested Flight Attitudes

	FLIGHT MACH NUMBER		
	0.35M	**0.6M**	**0.85M**
FLIGHT ATTITUDE AOA_AOSS	0_0	0_0	0_0
	0_8	0_8	0_8
	0_16	0_16	0_16
	8_8	8_8	8_8
	8_16	8_16	8_16
	16_8	16_8	16_8
	8_0	8_0	8_0
	16_0	16_0	16_0
	16_16	16_16	16_16

The change from one condition to the other was communicated into the solver's settings by changing the boundary conditions imposed on the outer boundaries of the Computational Domain. So, the flight Mach number and the attitude of the Aircraft (AOA and AOSS) were all defined by setting accordingly the Mach number and the direction, in reference to the X, Y and Z axis, of the flow entering the computational domain.

Figure 19 below presents the predicted contours of static temperature, static pressure and Mach number for the flight condition of 0.6M with 0˚ AOA and 0˚ AOSS.

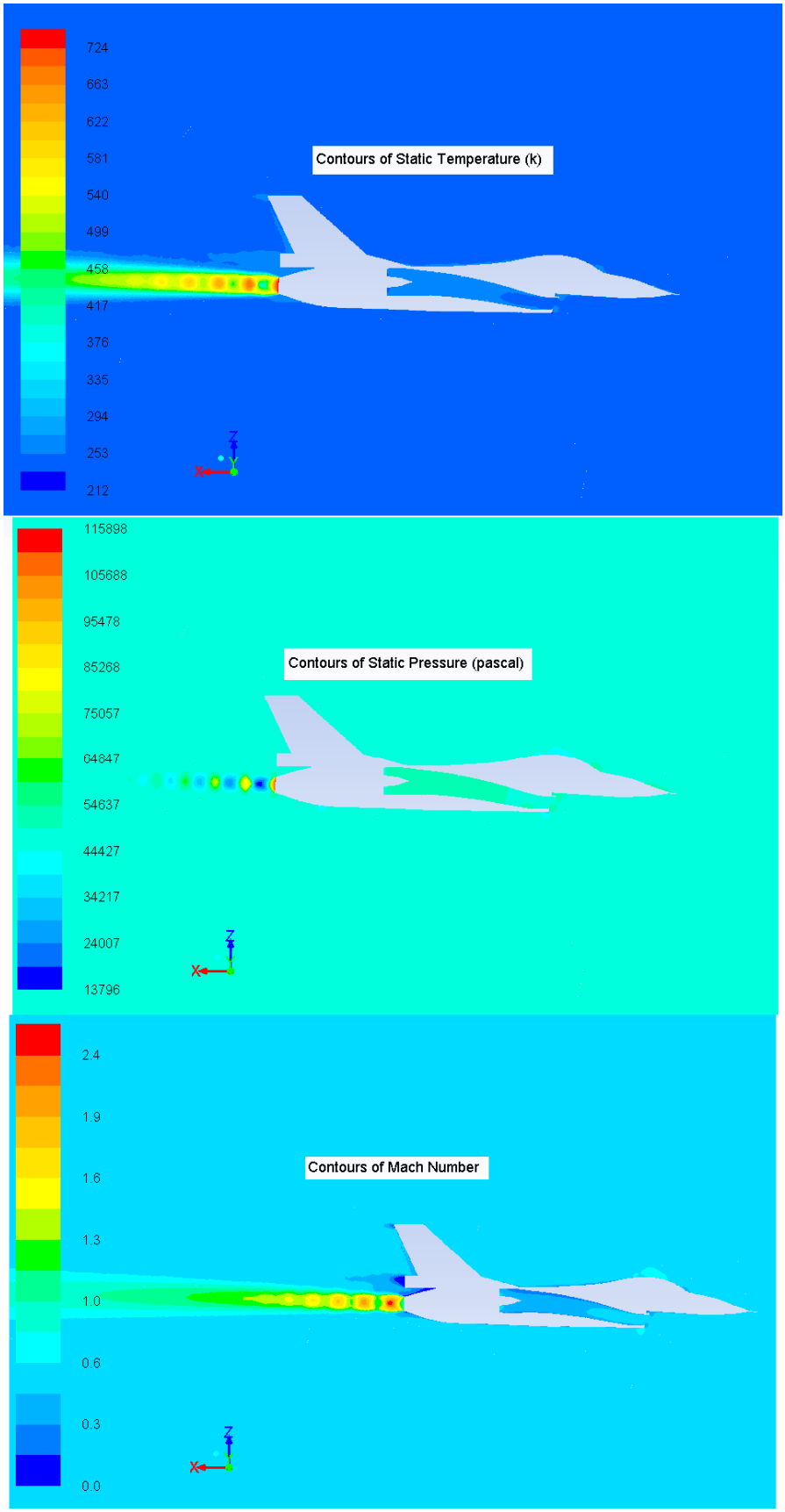

Fig. 19 Predicted Results for the 0.6M Flight with 0˚ AOA and 0˚ AOSS

From these figures, the diffusion of the flow inside the intake can be observed and also just after the nozzle's exit the presence of the shock cells can be noticed.

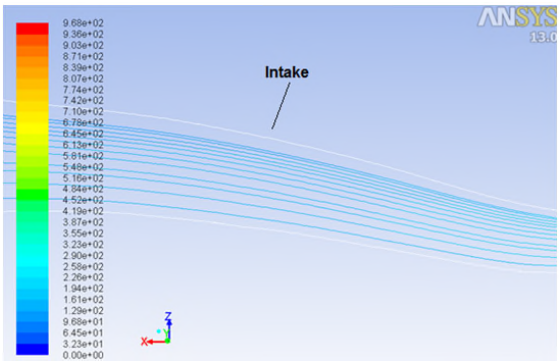

Fig. 20 Flow Pathlines Inside the Intake

7.1 Intake Flow Field Results

Figures 20 and 21 present in terms of flow pathlines and velocity vectors respectively, a visualisation of the flow inside the intake at this flight condition. The predicted flow propagates smoothly through the duct without any flow reversals. Also the flow enters the intake around its lip without any separations.

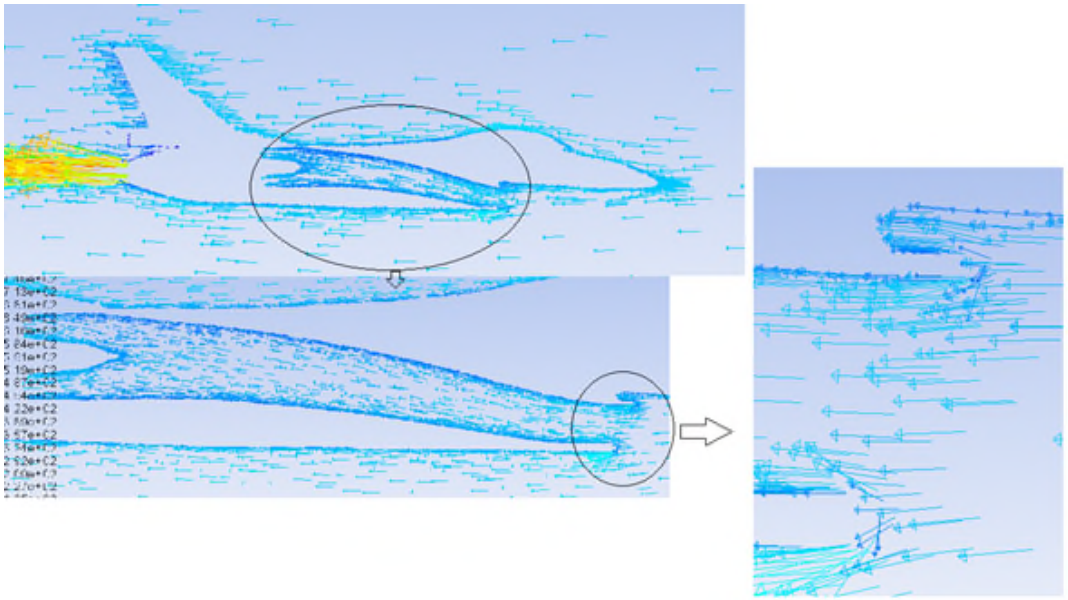

Fig. 21 Visualization of the Flow Inside the Intake in Terms of Velocity Vectors

There is a flight attitude though, that of 0.35M flight with 16˚ AOA and 0˚ AOSS, in which a small region of streamwise flow reversal was noticed at the lower side of the intake near to its entrance. At this specific flight attitude the lower side of the intake becomes ''shielded'' to the incoming flow, due to the increased AOA. As a result the flow has a lower velocity at this point comparing to the rest of the intake.

This low velocity flow as it travels through the intake, has to both follow the intake's curvature and overcome the adverse pressure gradient due to the flow diffusion that occurs after the throat of the intake. Its energy though is not sufficient to accomplish these tasks and eventually reverses. This reversed flow area which does not exist at the higher flight Mach number attitudes, is presented in fig. 22.

7.2 Investigation of the Intake's Flow Field

Figure 23 below presents the total pressure distribution at the AIP for the flight attitudes of 0.35M, 0.6M and 0.85M with 0° AOA and 0° AOSS. What can be observed in this figure is that as the flight Mach number increases the high pressure area resembles the shape of the intake's ''mouth'' and it migrates towards the lower part of the AIP.

To better investigate the airflow in the intake duct, four cross stream planes were created across the intake and with the aid of these planes the propagation of different flow parameters was observed. Figure 24 presents the progress of total pressure across the intake for the three flight attitudes (0.35M, 0.6M and 0.85M with 0° AOA and 0° AOSS). As it can be seen on this figure the low total pressure flow develops from top to the centre and in the last plane, the one that is closer to the AIP, the high total pressure is around the centre. As the flight Mach number increases the high total pressure area becomes smaller and it migrates towards the lower part of the AIP.

One of the reasons inducing the change of the total pressure is the development of secondary flow which is created due to the curvature of the intake. As soon as the airflow enters the intake it is diverted upwards due to the curvature of the intake creating thus secondary flow. Figure 25 presents this flow in the four cross stream planes for the flight attitude of 0.85M flight with 0° AOA and 0° AOSS. This figure accompanied by fig. 26 which presents the propagation of the static pressure across the intake cross stream planes provide an explanation on the direction and the magnitude of the secondary flow.

In the first plane (Plane A) the static pressure is higher at the sides due to the intake's shape at that plane in conjunction with its gradual transition to a circular shape downstream. A pressure gradient is created which gives rise to a flow motion towards the centerline of the plane. In plane B the secondary flow has become more severe since up to that plane the flow has gone through the first bend of the intake and it has been diverted towards the upper part of the intake. The secondary flow at that plane is slightly mitigated by the pressure gradient that has been created with higher static pressure at the top than at the lower part of the intake, as it can be observed in fig. 26. As the flow propagates furthermore and it passes through the second bend

of the intake which is in the opposite direction, the secondary flow alleviates even more and in plane D is at a much lower level than it was in the previous ones.

In lower Mach number flights the core flow has more time to interact with the low momentum boundary layer flow and to finally increase its low velocity. As a result in lower Mach number flights the high total pressure area in plane D is greater comparing to a high Mach number flight.

When the incoming flow enters the intake at an AOA it ends up on the AIP having the total pressure distributed in the way presented in figures 27 and 28. The former presents the total pressure distribution on the AIP when the airframe is exposed to an incoming flow with 8˚ AOA whereas the latter presents the same results for the 16˚ AOA. As it can be observed in these figures the high pressure area is again confined in the centre and migrates towards the lower side of the AIP as the flight Mach number increases. The low pressure area though, located at the lower part of the AIP, becomes more pronounced. Also, the lower the flight Mach number the more severe this low total pressure area seems to be.

At these flight attitudes the lower side of the intake becomes ''shielded'' to the incoming flow. As a result the flow moving adjacent to that wall has a lower velocity. This lower momentum flow is more sensitive to the pressure gradient due to the boundary layer build up as the flow propagates inside the intake. At higher flight Mach numbers the velocity of the flow near the wall is higher which is translated in a less severe low total pressure area on the AIP.

When the AOA increases, the flow neighbouring the lower side of the intake moves with an even lower velocity. This lower velocity flow is translated into a more intense low pressure area at the lower side of the AIP. This can be visualized in fig. 28 that presents the total pressure distribution at the AIP for the flight attitudes with 16˚ AOA and 0˚ AOSS.

In the case of an incoming flow at an AOSS the low pressure area on the AIP migrates to the side, at the 3 o'clock location, as it can be observed in figures 29 and 30. It is this part of the intake that becomes ''shielded'' to the incoming flow and consequently has lower flow velocity. This low pressure area becomes more pronounced at higher AOSS.

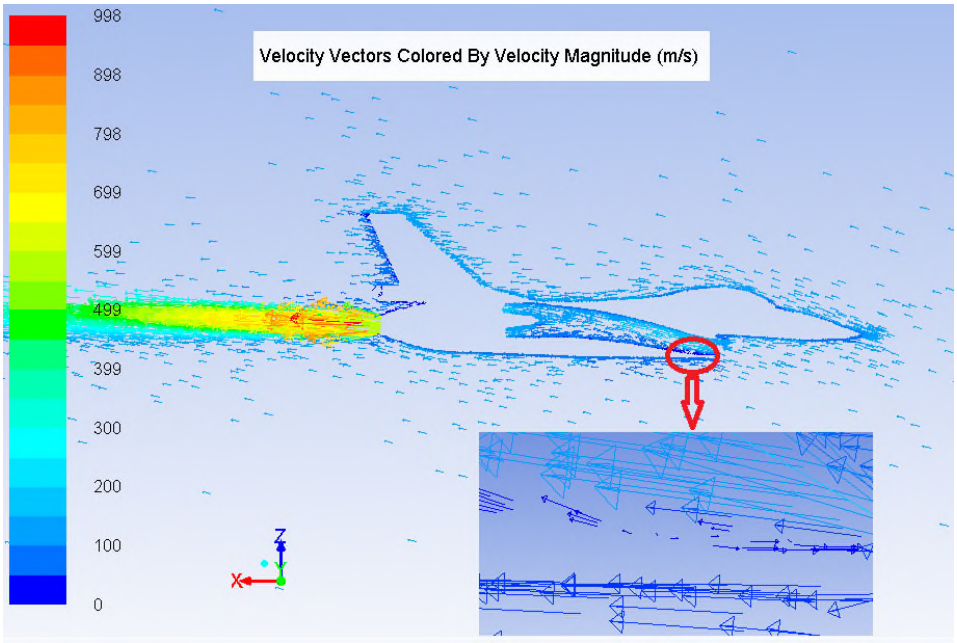

Fig. 22 Reversed Flow Area at the Flight Attitude of 0.35M with 16˚AOA and 0˚AOSS

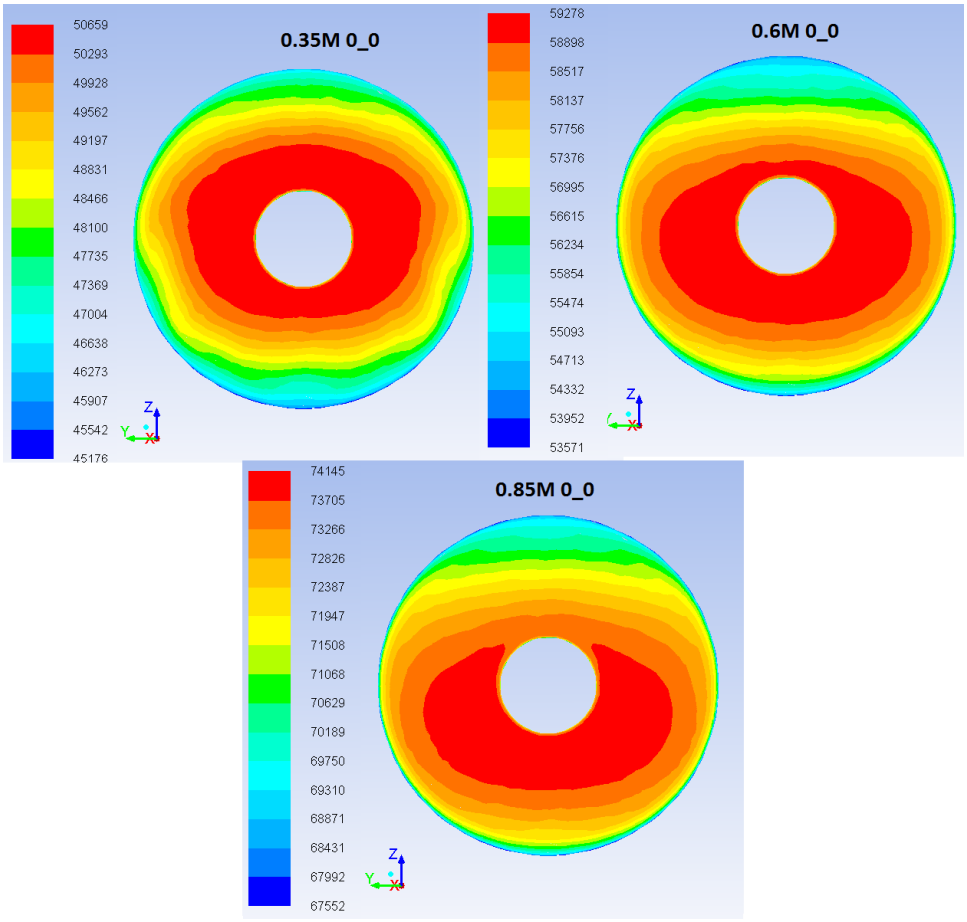

Fig. 23 Total Pressure Profiles at the AIP for the 0.35M, 0.6M and 0.85M Flights with 0˚AOA and 0˚AOSS

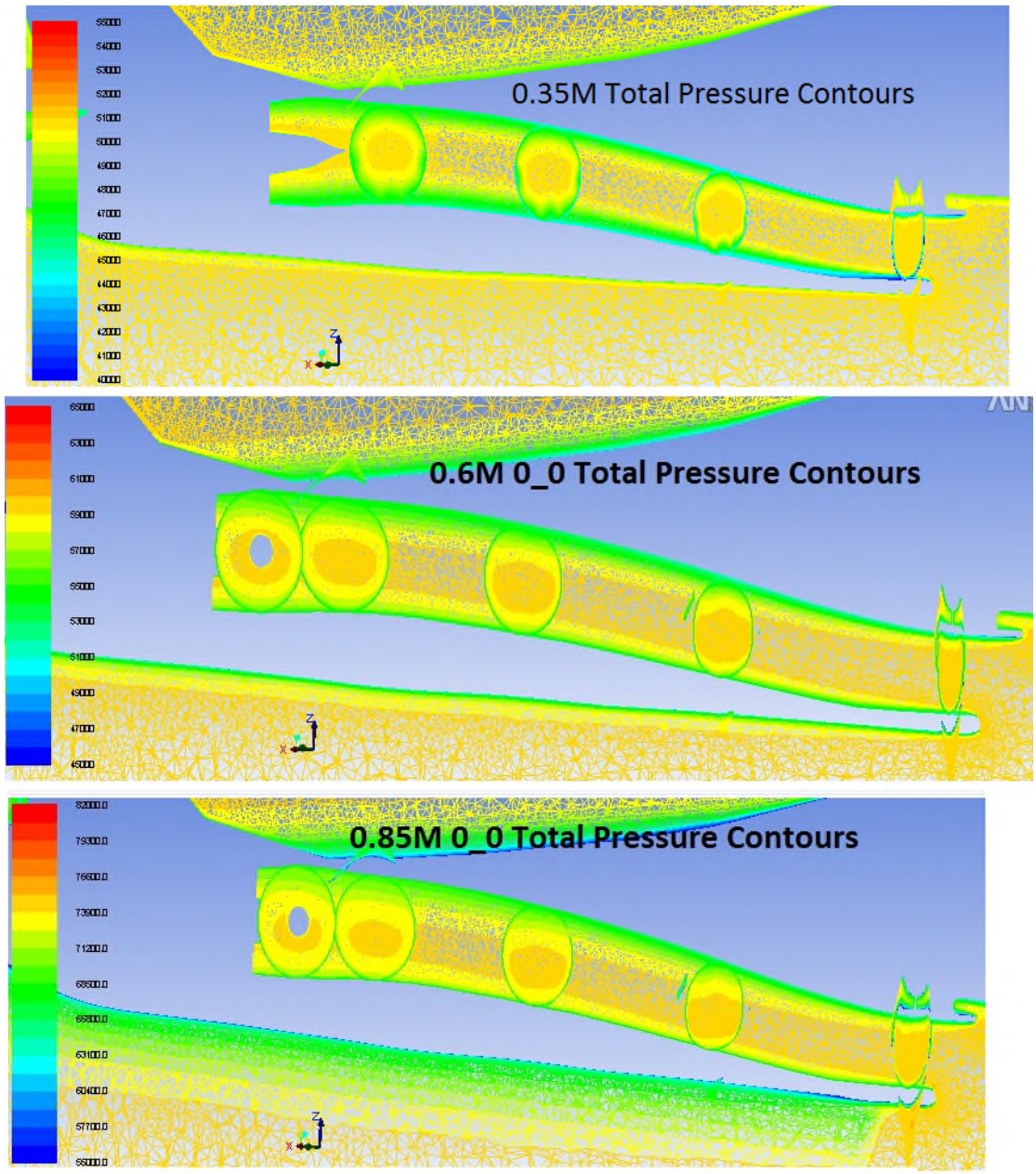

Fig. 24 Total Pressure Contours Across the Intake for the 0.35M, 0.6M and 0.85M Flights with 0˚AOA and 0˚AOSS

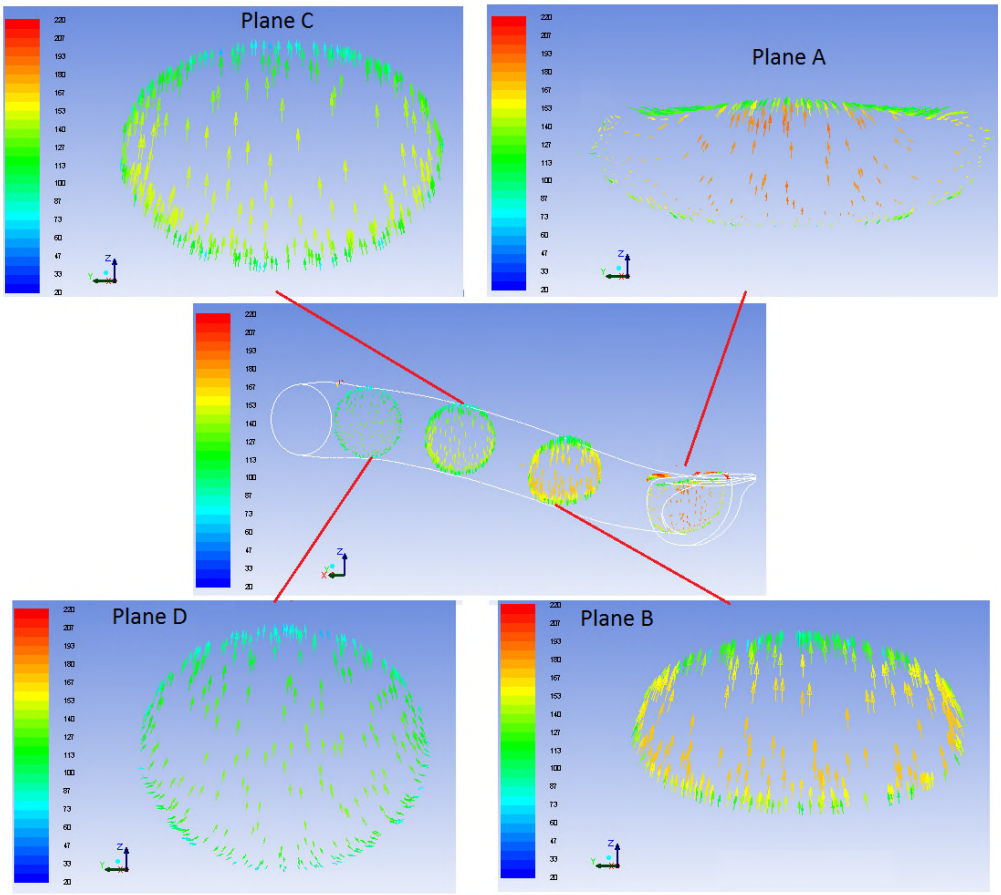

Fig. 25 Secondary Flow on the Cross Stream Planes Across the Intake for the 0.85M Flight with 0˚ AOA and 0˚ AOSS

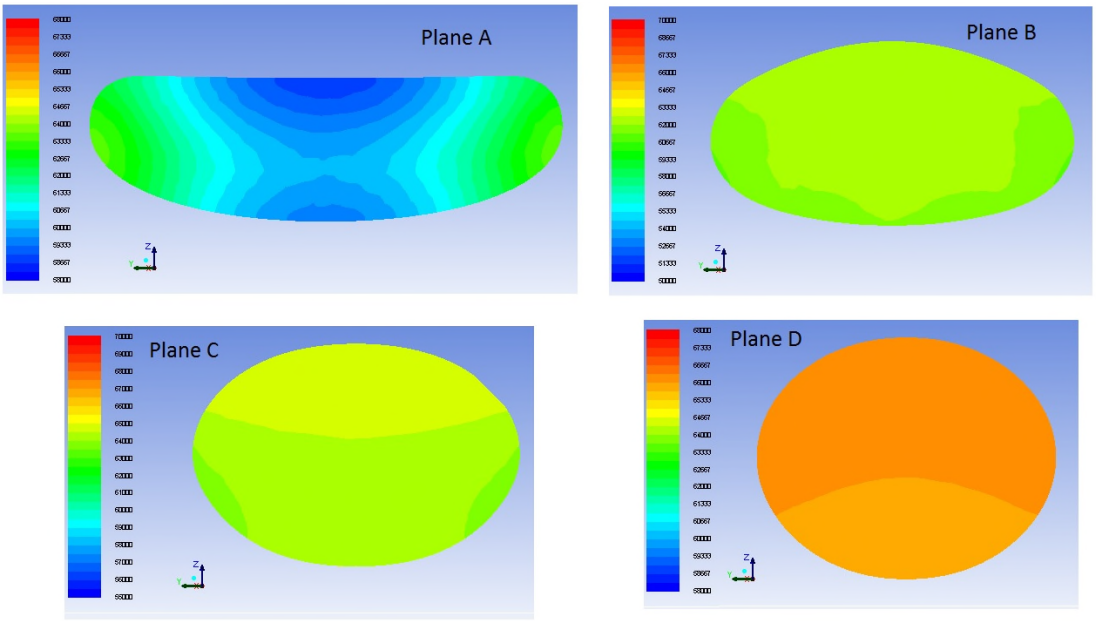

Fig. 26 Static Pressure Contours at the Cross Stream Planes Across the Intake for the 0.85M Flight with 0˚ AOA and 0˚ AOSS

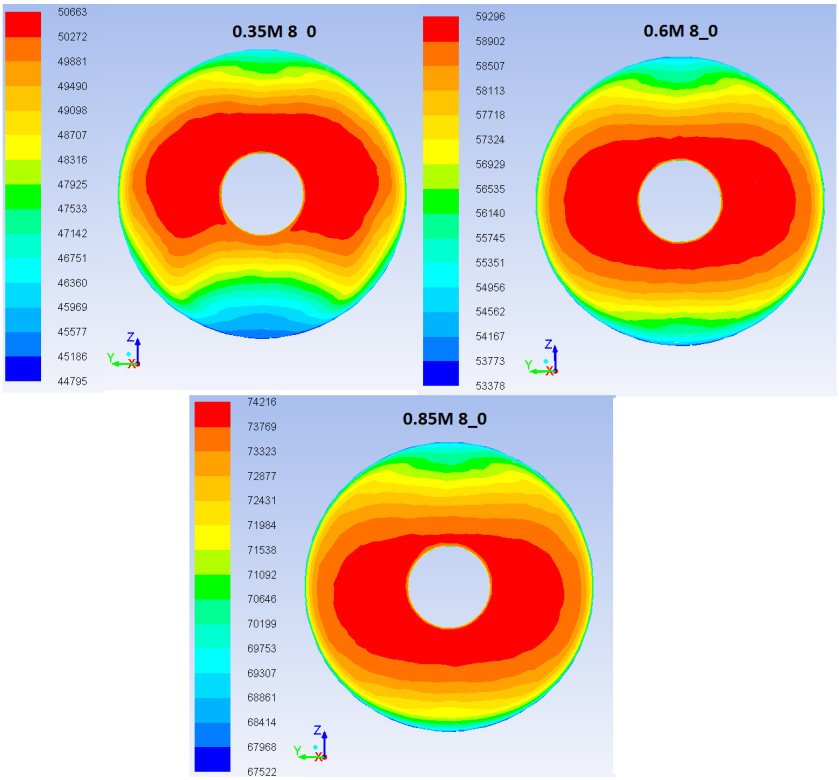

Fig. 27 Total Pressure Profiles at the AIP for the 0.35M, 0.6M and 0.85M Flights with 8˚AOA and 0˚AOSS

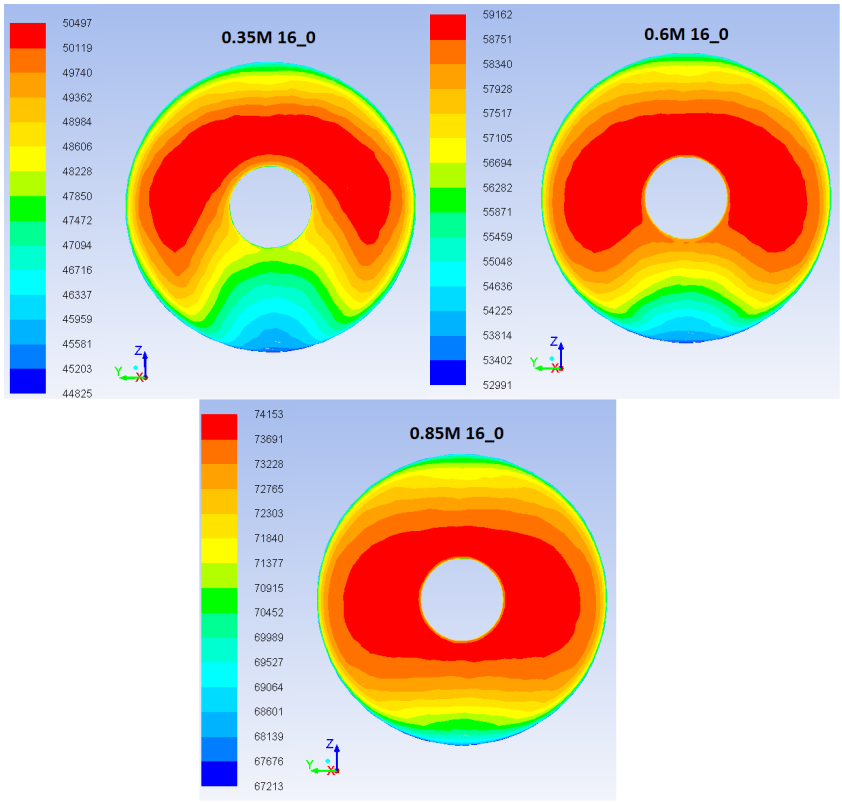

Fig. 28 Total Pressure Profiles at the AIP for the 0.35M, 0.6M and 0.85M Flights with 16˚AOA and 0˚AOSS

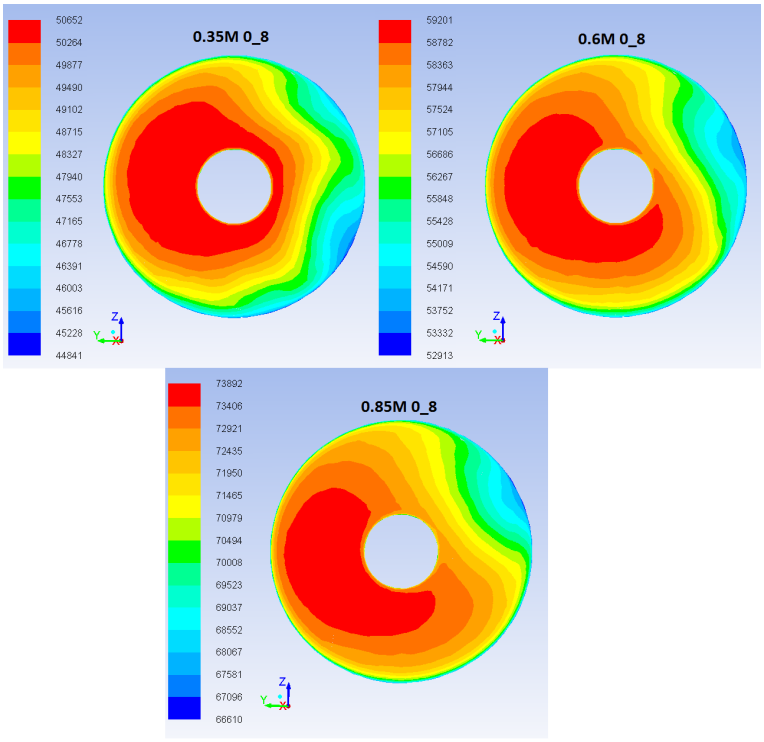

Fig. 29 Total Pressure Profiles at the AIP for the 0.35M, 0.6M and 0.85M Flights with 0˚AOA and 8˚AOSS

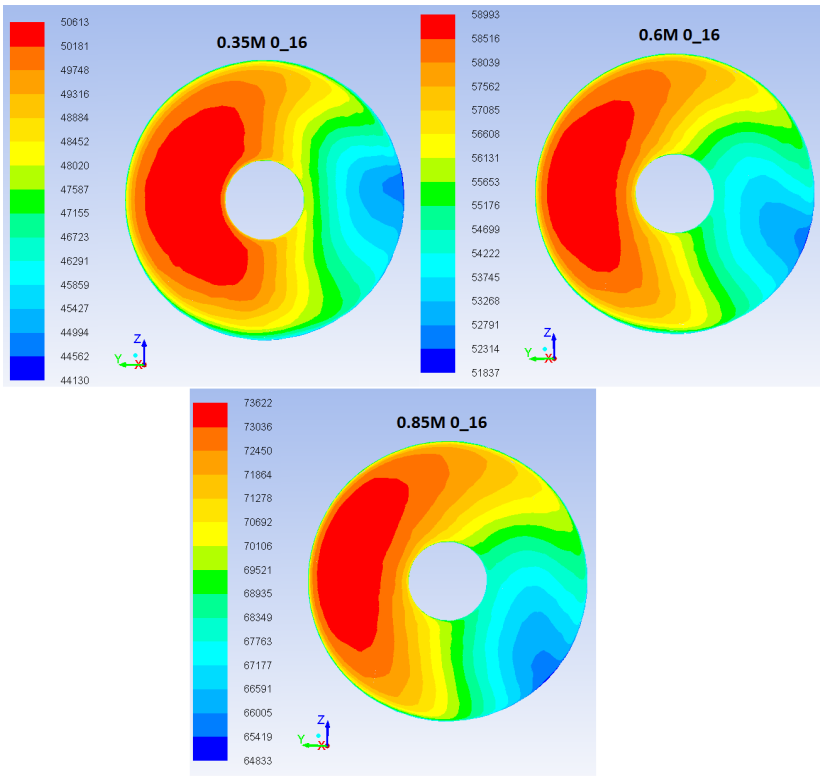

Fig. 30 Total Pressure Profiles at the AIP for the 0.35M, 0.6M and 0.85M Flights with 0˚AOA and 16˚AOSS

7.3 Intake pressure recovery

The intake's pressure recovery as the ratio of the area weighted average of the total pressure at the AIP to the total pressure at the entry of the intake was also calculated for all the tested conditions and the results are presented in Table 4.

Table 4 CFD Predicted Values of Intake Pressure Recovery

ATTITUDE	FLIGHT MACH NUMBER		
AOA_AOSS	**0.35M**	**0.6M**	**0.85M**
0_0	0.973	0.977	0.974
0_8	0.970	0.972	0.968
0_16	0.959	0.953	0.945
8_8	0.968	0.975	0.975
8_16	0.959	0.962	0.960
16_8	0.965	0.973	0.975
8_0	0.971	0.979	0.978
16_0	0.968	0.975	0.977
16_16	0.958	0.961	0.962

Among the tested conditions the intake performs worst in terms of Pressure Recovery at the flight attitude of 0.85M with 0˚ AOA and 16˚ AOSS. And this was expected since the Total pressure profile at the engine's face from this specific attitude presents the greatest dark shaded area in fig 21. On the contrary, when the aircraft is supposed to fly at 0.6M with 8˚ AOA and 0˚ AOSS the intake presents the best value of pressure recovery.

8. CONCLUSIONS

The process described herein is a part of a wider study [11], [21] the main objective of which is to estimate how the installed gas turbine engine's performance is affected by the aircraft's flight attitude. The airflow reaching the engine's face was predicted for each one of the examined flight attitudes and a total pressure profile at this plane was obtained.

The created CFD model comprises of military aircraft geometry (inspired by the General Dynamics/Lockheed Martin F-16 aircraft) which is supposed to be equipped with a gas turbine engine (F100-PW-229-like). The predicted results have been validated through a comparison with experimental ones and they are in good agreement.

As it can be seen from the resulted Total Pressure profiles at the intake's exit the airflow reaching the engine's face is not uniform at all. Depending on the aircraft's flight attitude the quality of the airflow that enters the engine varies significantly.

The predicted profiles present a variation in Total Pressure which becomes more prominent at the flight attitudes that an AOSS has been induced.

The intake's Pressure Recovery which is a performance parameter of the intake, as it was expected follows these variations and its minimum values occur at the attitudes with the greatest AOSS.

The selected Turbulence model comprises a source of possible uncertainty in the predicted results. The standard wall functions selected

may have left unpredicted the occurrence of flow separations inside the intake at specific flight attitudes. Another source of possible uncertainty is the extension of the flow domain behind the intake's exit with the addition of a simple accelerating duct and not with the FAN component itself. However as it has been already explained in detail, the complexity of the geometry left no other choices than the selected approaches.

9. REFERENCES

1. ANSYS FLUENT 12.0, Theory Guide, ANSYS Inc, 2009-01-23
2. Palmer J. R., 1990, The TURBOMATCH Scheme For Aero/Industrial Gas Turbine Engine Design Point/Off Design Performance Calculation, SME, Thermal Power Group, Cranfield University.
3. G. W. Huband, J. S. Shang, M. J. Aftosmis, 1990, Numerical Simulation of an F-16A at Angle of Attack, J. Aircraft, Vol. 27, No 10.
4. Reue, G. L., Doberenz, M. E., Wilkins, D. D., 1976, Component Aerodynamic Load from 1/9-Scale F-16A Loads Model, General Dynamics Report 16PR316, Fort Worth, Tex., May 1976.
5. http://www.airwar.ru/other/draw/f16cb52_aiv.html, 1-5-2014
6. http://www.aerospaceweb.org/aircraft/fighter/f16/, 1-5-2014
7. http://xyextract-graph-digitizer.soft112.com/, 1-5-2014
8. https://www.sharcnet.ca/Software/Gambit/index.htm, 14-7-14
9. Hawkins J. E., 1974, YF-16 Inlet Design and Performance, AIAA/SAE 10th Propulsion Conference, San Diego, California, Oct 21-23 1974, AIAA 74-1062
10. András Sóbester, 2007, Tradeoffs in Jet Inlet Design: A Historical Perspective, JOURNAL OF AIRCRAFT, Vol. 44, No. 3, May–June 2007
11. T. Triantafyllou, T. Nikolaidis, M. Diakostefanis, P. Pilidis, 2015, *Effect of Inlet Flow Distortion on Installed Gas Turbine Performance,* Submitted for Publication In Journal of Propulsion and Power, Nov 2015, 2015-10-B36051
12. Kenneth C. Weston, 1992, ENERGY CONVERSION-The ebook, Ch. 5,
13. Seddon J., Goldsmith E.L., 1999, INTAKE AERODYNAMICS, Blackwell Science ltd.
14. Delaunay, B., 1934, Sur la sphere vide, Izvestia Akademii Nauk SSSSR, Mathematical and Natural Sciences Division, No. 6, 793-800
15. U.S. Standard Atmosphere, 1976, NASA-TM-X-74335
16. Jane's AERO-ENGINES, 2007, Issue 21, Jane's Information Group..
17. A. S. Lee, R. Singh, S. D . Probert, 2009, Modelling of the Performance of a F100-PW229 Equivalent Engine under Sea-level Static Conditions, 45th AIAA/ASME/SAE/ASEE Joint

Propulsion Conference & Exhibit, AIAA 2009-5018.

18. Salim .M. Salim, S.C. Cheah, 2009, Wall Y+ Strategy for Dealing with Wall-bounded Turbulent Flow, Proceedings of the International Multi Conference of Engineers and Computer Scientists 2009 Vol II, IMECS 2009, March 18 - 20, 2009, Hong Kong
19. Gilles Eggenspieler, Turbulence Modelling, ANSYS presentation, May 14, 2012
20. ANSYS FLUENT User's Guide, Release 14, 2011
21. T. Triantafyllou, T. Nikolaidis, M. Diakostefanis, P. Pilidis, 2015, *Total Pressure Distortion Levels at the Aerodynamic Interface Plane of a Military Aircraft*, The Aeronautical Journal, Volume 119 No 1219, September 2015